Dynamic Performance of a Grid-Tied Solar PV with Unbalance Control

Abdulhakim Alsaif, *Student Member, IEEE,* Zhixin Miao, *Senior Member, IEEE*

***Abstract*—The main objective of this work is to evaluate the influence of an unbalance mitigation scheme on a grid-tied PV system's dynamic performance through electromagnetic transient (EMT) simulation. The test bed has been built in MATLAB/SimScape environment. A PV inverter control without unbalance mitigation capability and another with such capability have been implemented in the test bed. EMT simulation experiments show that the unbalance control not only effectively enhances transient stability of the grid but also limits the injection of the negative-sequence current into the grid. The benefits of the control are presented through two case scenarios, single-line-ground fault and unbalanced grid voltage dip.**

***Index Terms*—Solar photovoltaic (PV) grid integration, unbalance control, fault analysis**

I. Introduction

With high penetration of grid connected PV converters, operation of these converters under non-ideal grid conditions such as asymmetrical short circuit faults is a critical issue to be examined [1]. Under these circumstances, real-world field recorded data from Dominion Energy show that grid-connected solar PV inverters are designed to suppress the injection of negative-sequence current into the grid [2].

When the negative-sequence current is subdued in a grid-connected voltage-source converter (VSC), its order typically is commanded to be zero. Consequently, this setting leads to fluctuation in the total instantaneous power and the dc-link voltage due to the interaction between positive-sequence current and negative-sequence grid voltage.

A more practical unbalance mitigation control design is to eliminate power ripples. This is achieved by regulating not only the positive-sequence current but also the negative-sequence current based on computing. Such concept has been demonstrated in the literature for VSC converters, e.g., [3], [4], and for type-3 wind turbines [5].

Many papers in the literature assume that the outer loops of the VSC control are implemented in the PQ regulation mode as shown in [6]. On the other hand, PV regulation mode (dc-link, and ac voltage regulation) is significantly more prevalent in solar PV grid-connected converters. Therefore, in the current paper, dc-link and ac voltage controls are adopted along with the unbalance control on grid-connected solar PV system to mitigate ripples in the total three-phase power and the dc voltage.

In the current control implementation level, different methods have been introduced.

The double synchronous reference frame (DSRF) control is an effective method to control both sequence currents [3], [7]. The decoupled DSRF (DDSRF) is an enhanced technique of DSRF to eliminate 2ω ripples from each sequence transformed dq currents [8]. Both DSRF and DDSRF are based on two control loops using PI controllers for each sequence frame.

The second implementation method is based on the stationary frame. Unbalanced currents can be regulated in a single control loop using proportional-resonant (PR) control [9], [10].

In this paper, the unbalance control strategy with the goal to eliminate ripples in the total power is implemented in the stationary frame via PR current control for a three-wire three-phase solar PV's system, as shown in Fig. 1. A grid voltage dip and asymmetrical fault on the transmission line are applied to analyze the unbalance control's influence on the system's transient behavior. To demonstrate negative-sequence current regulation and real power ripples mitigation, a case without unbalance control scheme is also constructed for comparison.

The ensuing of sections are organized as follows. Section II presents the EMT test bed and the conventional control structure of an PV inverter without the capability of unbalance mitigation. Section III presents the details of unbalance control implementation. Case studies and simulation results are provided in Section IV. Section V summarizes the paper's main conclusions.

II. EMT Test Bed and the PV Inverter Control Structure

A. EMT test bed

The EMT test bed used in this study is shown in Fig. 1. The test bed is a three-phase grid-connected PV system developed in MATLAB/SimScape environment. The PV farm consists of four parallel PV arrays, and each array generates a maximum power of 100 kW at 1000 W/m^2 sun irradiance. The PV arrays are interfaced a two-level VSC through a DC/DC boost converter for each array. The DC/DC converters are operated at maximum power point tracking (MPPT)-perturb and observe algorithm, to regulate the PV array voltage (V_{pv}) at 260 V. The VSC system is connected to a line through two Y-ground Y-ground transformer step up the 260 V to a 25 kV line and then to a 120 kV grid. The parameters of the test bed are presented in Table I.

B. PLLs for Grid Synchronization System

Two phase looked loops (PLL) techniques are employed in this study due to the grid synchronization system's need. The grid voltage phase angle is usually detected by a conventional synchronous reference frame PLL (SRF-PLL). It is operated usually along with conventional control for balanced cases

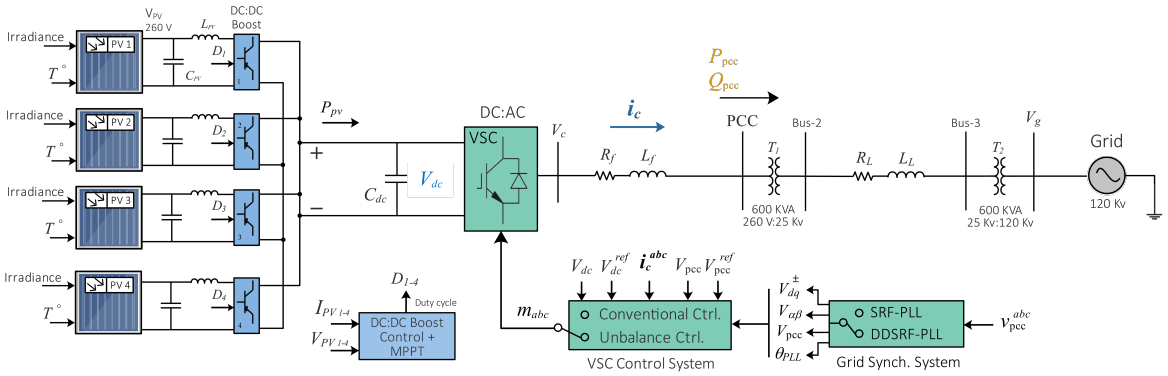

Fig. 1: The EMT testbed: 400-kW solar photovoltaic system connected to a three-phase grid, with different VSC control systems.

Table I: The PV testbed and VSC system control parameters.

	Description		Symbol	Value
Grid side	Transmission line		R_L, X_L	$X_L/10$, 0.2 pu
	System frequency		f	60 Hz
PV side	power base		S	400 kVA
	ac voltage base		V_{ac}	260 V, 25 Kv
	dc voltage base		V_{dc}	500 V
	VSC filter		R_f, X_f	$X_f/50$, 0.156 pu
	dc-link capacitor		C_{dc}	0.02 F
	PV inductor/capacitor		L_{pv}, C_{pv}	5 mH , 100 μF
VSC control system	Outer voltage loops	DC-voltage Ctrls	k_{pp}, k_{ip}	1 , 100
		PCC-voltage Ctrls	k_{pv}, k_{iv}	1 , 400
	Inner current loops	Conv. Ctrls	k_{pi}, k_{ii}	0.3 , 5
		Unbalance Ctrls	k_p, k_r	0.32 , 3.32
	SRF-PLL DDSRF-PLL	PI controllers	k_p, k_i	60 , 1400

[11]. However, when a grid subjects to unbalance, this PLL is no longer properly detecting the angle due to voltage ripples of its input. Thus, as an alternative, a decoupled DSRF-PLL is suitable to be used with the unbalance control. This kind of PLL is not only able to extract the phase angle accurately, but also to cancel out ripples form its voltage input [3].

C. Conventional Control Structure

This subsection presents the inner control, sequence reference currents generation for unbalance control, and the outer loop regulators.

Firstly, the conventional inverter control implemented in a PLL enabled dq frame is presented in Fig. 2. The inverter control regulates the dc voltage and ac voltage. The d-axis current control is generated by the dc-link voltage control while the q-axis current order is generated by the ac voltage control. The inner current control is implemented in the dq frame using PI controller to track the current orders. This control structure is a well known structure and have been thoroughly discussed in the classic book on VSC [12] as well as our own paper [13].

III. Unbalance Control Implementation

Next, we examine the unbalance control implementation, shown in Fig. 3.

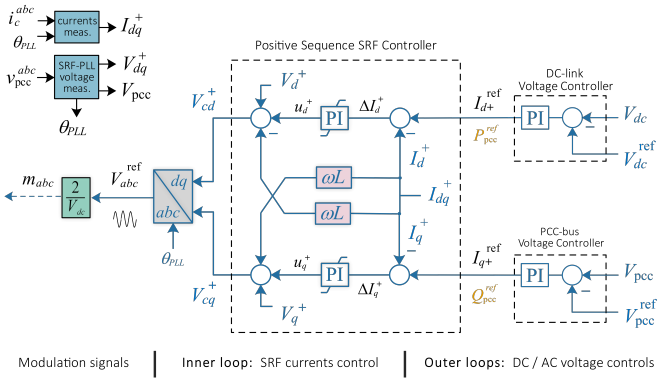

Fig. 2: Conventional control structure block of a grid-connected VSC system, namely as a conventional grid-connected control using dq reference frame [1].

A. Unbalance Control: Inner Current Control Loop

The three-phase dynamic equations of VSC AC system is expressed in abc frame as follows.

$$L_f \frac{\mathrm{d}i_{c_{abc}}}{\mathrm{d}t} = -R_f\, i_{c_{abc}} + v_{c_{abc}} - v_{\mathrm{pcc}_{abc}} \tag{1}$$

where $v_{c_{abc}}$, and $i_{c_{abc}}$ are three-phase output voltages and currents of the converter. $v_{\mathrm{pcc}_{abc}}$ is the voltages at Point of Common Coupling (PCC)-bus, respectively. $Z_f = R_f + jX_f$ is defined as filter impedance. (1) can be represented to space-phasor form as follows.

$$L_f \frac{\mathrm{d}\overrightarrow{I_c}}{\mathrm{d}t} = -R_f \overrightarrow{I_c} + \overrightarrow{V_c} - \overrightarrow{V}_{\mathrm{pcc}} \tag{2}$$

Eq. (2) can be then represented either in the stationary frame ($\alpha\beta$-frame) or synchronous reference frame (SRF) (dq-frame). At steady state, $\alpha\beta$ components are sinusoidal waveform, while dq components are DC signals.

Since each component in (2) is defined such as $\overrightarrow{i}_c = i_{c_\alpha} + j i_{c_\beta}$, (2) can be formed in $\alpha\beta$-frame by splitting it into real

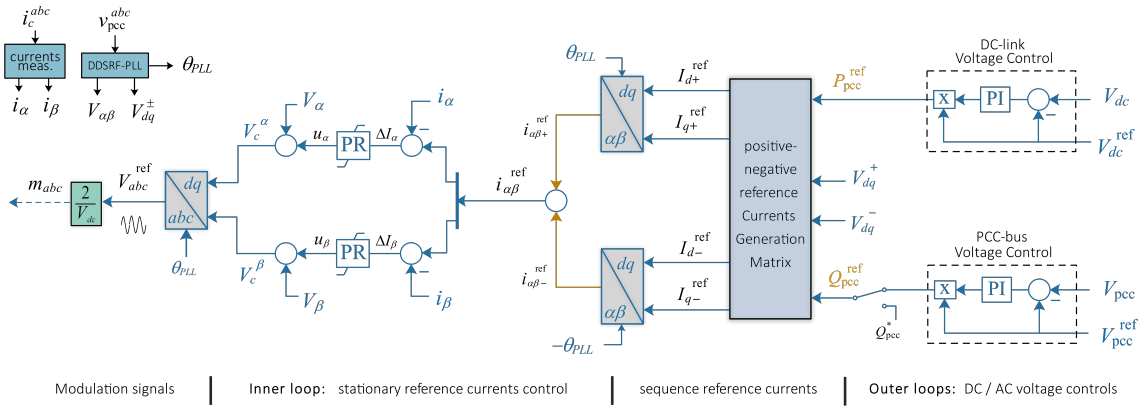

Fig. 3: Unbalance control structure block of a VSC in a grid-connected system.

and imaginary part as in (3) and (4).

$$L_f \frac{\mathrm{d}i_{c_\alpha}}{\mathrm{d}t} = -R_f\, i_{c_\alpha} + V_{c_\alpha} - V_{\mathrm{pcc}_\alpha} \tag{3}$$

$$L_f \frac{\mathrm{d}i_{c_\beta}}{\mathrm{d}t} = -R_f\, i_{c_\beta} + V_{c_\beta} - V_{\mathrm{pcc}_\beta} \tag{4}$$

Due to the sinusoidal signals of $\alpha\beta$-components, two proportional+resonant controllers (PR controllers) can track simultaneously $\alpha\beta$ current orders. As a result, the converter voltage can be regulated as:

$$V_{c_\alpha} = u_\alpha + V_{\mathrm{pcc}_\alpha},\ \ V_{c_\beta} = u_\beta + V_{\mathrm{pcc}_\beta} \tag{5}$$

$$\text{where}\ \ u_\alpha = (I_\alpha^* - I_\alpha)\left(k_p + \frac{2k_r}{s^2+\omega_0^2}\right)$$

$$u_\beta = (I_\beta^* - I_\beta)\left(k_p + \frac{2k_r}{s^2+\omega_0^2}\right)$$

Note that V_{c_α} and V_{c_β} are linearly proportional to the modulation signals m_α and m_β, respectively, by a proportionality gain of $V_{dc}/2$. A control diagram of PR controllers regulating sequence currents is illustrated in Fig. 3.

B. Unbalance Control: Positive-Negative Current Reference Generation

The $\alpha\beta$-frame current orders will be generated by a computing block. This computing is based on the complex power equation. The instantaneous complex power at PCC to be delivered in the grid is expressed in space-phasor as follows.

$$S_{\mathrm{pcc}} = \overrightarrow{V}_{\mathrm{pcc}}\, \overrightarrow{I}_c^{\,*} = P_{\mathrm{pcc}} + jQ_{\mathrm{pcc}} \tag{6}$$

The space vectors in (6) may be defined in double dq frames as the sum of positive and negative sequence vectors, such that, $\overrightarrow{V}_{\mathrm{pcc}} = V^+_{\mathrm{pcc}_{dq}} e^{j\omega t} + V^-_{\mathrm{pcc}_{dq}} e^{-j\omega t}$. Therefore, (6) can be rewritten as follow.

$$\begin{aligned} S_{\mathrm{pcc}} &= \left(V^+_{dq}\, e^{j\omega t} + V^-_{dq}\, e^{-j\omega t}\right)\left(I^+_{dq}\, e^{j\omega t} + I^-_{dq}\, e^{-j\omega t}\right)^* \\ &= \Big[P_0 + + \overbrace{P_{c2}\,\cos(2\omega t) + P_{s2}\,\sin(2\omega t)}^{P_{\mathrm{ripple}}}\Big] \\ &\quad + j\Big[Q_0 + \underbrace{Q_{c2}\,\cos(2\omega t) + Q_{s2}\,\sin(2\omega t)}_{Q_{\mathrm{ripple}}}\Big] \end{aligned} \tag{7}$$

where ω is the angular frequency. The notation "+" signifies the positive components rotating in counterclockwise, whose angle frequency is $\theta^+ = +\omega t$. The "−" denotes the negative components rotating in clockwise at $\theta^- = -\omega t$.

The real part of (7) represents the total instantaneous active power P_{pcc}, while the reactive power Q_{pcc} is represented by the imaginary part. P_0 and Q_0 are the average values of the instantaneous active and reactive powers, respectively. P_{c2}, P_{s2}, Q_{c2} and Q_{s2} are the magnitudes of the double frequency ripples of the instantaneous powers. Eq. (7) can be formed in a 6×4 matrix as.

$$\begin{bmatrix} P_0 \\ Q_0 \\ P_{c2} \\ P_{s2} \\ Q_{c2} \\ Q_{s2} \end{bmatrix} = \begin{bmatrix} V_d^+ & V_q^+ & V_d^- & V_q^- \\ V_q^+ & -V_d^+ & V_q^- & -V_d^- \\ V_d^- & V_q^- & V_d^+ & V_q^+ \\ V_q^- & -V_d^- & -V_q^+ & V_d^+ \\ V_q^- & -V_d^- & V_q^+ & -V_d^+ \\ -V_d^- & -V_d^- & V_d^+ & V_q^+ \end{bmatrix} \begin{bmatrix} I_d^+ \\ I_q^+ \\ I_d^- \\ I_q^- \end{bmatrix} \tag{8}$$

Because Q_{c2} and Q_{s2} do not affect the active power oscillations; they can be ignored. Thus, they do not need to be controlled. Hence, if the real power ripples are to be eliminated, with the PCC voltage's positive-, negative-sequence known, the current references can be found as follows.

$$\begin{bmatrix} I_d^+ \\ I_q^+ \\ I_d^- \\ I_q^- \end{bmatrix}^{\mathrm{ref}} = \begin{bmatrix} V_d^+ & V_q^+ & V_d^- & V_q^- \\ V_q^+ & -V_d^+ & V_q^- & -V_d^- \\ V_d^- & V_q^- & V_d^+ & V_q^+ \\ V_q^- & -V_d^- & -V_q^+ & V_d^+ \end{bmatrix}^{-1} \begin{bmatrix} P_0 = P_{\mathrm{pcc}}^{\mathrm{ref}} \\ Q_0 = Q_{\mathrm{pcc}}^{\mathrm{ref}} \\ P_{c2} = 0 \\ P_{s2} = 0 \end{bmatrix} \tag{9}$$

To obtain the sequence current references orders, (8) can be reduced to a 4×4 matrix since Q_{c2} and Q_{s2} are neglected, then by taking the inverse of (7), as given in (9). The power ripples (P_{c2}, P_{s2}) are set to zero to achieve proper reference currents. P_0 and Q_0 are defined in this study as $P_{\mathrm{pcc}}^{\mathrm{ref}}$ and $Q_{\mathrm{pcc}}^{\mathrm{ref}}$, which are acquired from the outer loops, respectively, as discussed in the following section,

Note that the dq reference orders are transferred into $\alpha\beta$-frame. Thus, the sum of $i_{\alpha\beta+}^{\mathrm{ref}}$ and $i_{\alpha\beta-}^{\mathrm{ref}}$ provides the combined

reference commands, $i_{\alpha\beta}^{\text{ref}}$, to be implemented to the inner loop controllers.

C. Unbalance Control: Outer Loops: dc and ac voltages controllers

A challenge of implementation is how to determine the power references: $P_{\text{pcc}}^{\text{ref}}$ and $Q_{\text{pcc}}^{\text{ref}}$. The outer loop control regulated dc voltage and ac voltage. Thus, only dc voltage reference and ac voltage reference can be treated as given.

In the conventional control shown in Fig. 2, the outer control generates the dq-axis current references. Note that the dq-axis currents at steady state are associated to PQ. Hence, it is contemplated that the PQ references can be generated by the outer control. This is the significant difference of the unbalance control versus the conventional control. This strategy of real power reference generation through dc-link voltage control has also been used in [14].

IV. Case Studies & Simulation Results

Two case scenarios are demonstrated to evaluate the 400-kW PV dynamic performance under unbalance grid conditions, which are single-line-ground (SLG) fault and grid voltage dip. in test bed 1, the conventional control mode is used, while testbed 2 uses the unbalance control mode. In both testbeds the set-points of the dc-link and ac voltages reference (V_{dc}^{ref}, $V_{\text{pcc}}^{\text{ref}}$) are initially ordered at 1 pu. An average model for the VSC is adopted for fast simulation speed.

A. Case-1: Performance of the systems during single-line-ground fault

A SLG fault is applied on the transmission line at t = 0.6 sec for duration of two cycles. A dynamic performance comparison of the conventional control and unbalance control during the disturbance is shown in Fig. 4. Results show time domain responses of three-phase voltage at Bus-2, dc-link voltage, PCC instantaneous active power, voltage magnitude at PCC-bus, and the system frequency.

Due to the fault, high transients appear in the real power when the conventional control is used. However, the unbalance control is able to smoothen these transients.

The symmetrical sequence components of the faulty three-phase currents are shown in Fig. 5. It can be seen that overcurrent can be significantly reduced by the unbalance control.

Remark: Compared to the conventional control mode, the use of unbalance control mode enhances relatively the dynamic performance of the system by reducing overcurrent and ripples in real power, dc-link voltage, voltage, and measured frequency.

B. Case-2: Performance of the systems during grid voltage dip

In this case, the dynamic performance of the 400-kW PV system is analyzed when the grid subjects to a voltage dip. The V_g in phase a falls to 0.7 pu during the time period from 0.6 sec to 0.8 sec.

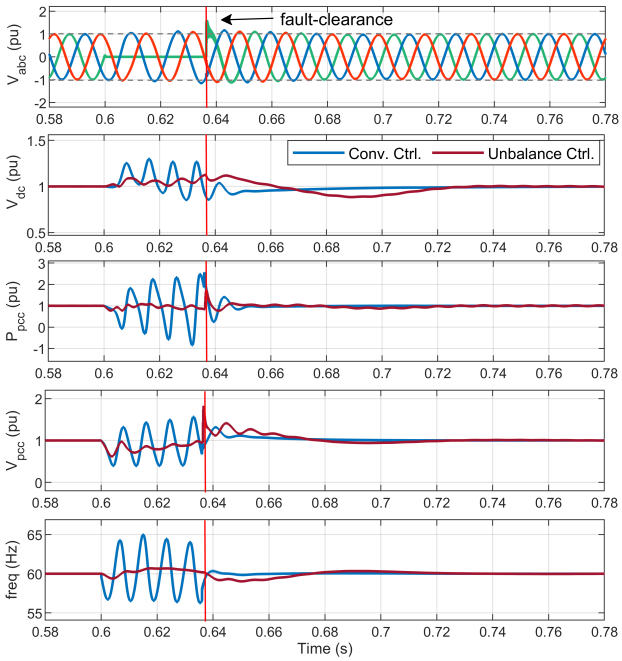

Fig. 4: Case 1: time domain simulation responses of SLG fault at 0.6 sec. From top to bottom, three-phase voltage, dc-link voltage, PCC active power, PCC-bus voltage, and system frequency.

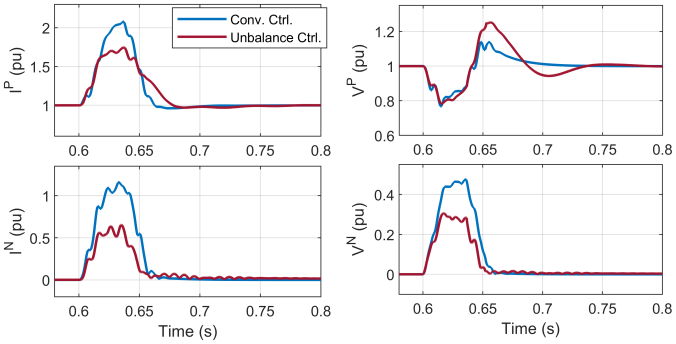

(a) I^+ and I^- (b) V^+ and V^-

Fig. 5: Case 1: dynamic responses of the symmetrical sequence current and voltage components, due to SLG fault.

During the voltage dip, as illustrated in Fig. 6, it is evident that the conventional control lacks the ability to cancel out the frequency ripples of the real power and the dc voltage. In contrast, when the VSC system is operated in unbalance control, it ensures a stable operation of the system to deliver a smooth real power into the grid by mitigating the oscillations. Also, since DDSRF-PLL operated along with the unbalance control, it is able to eliminate the ripples of the ac voltage and system frequency.

The time-domain responses of the positive- and negative-sequence currents (I^+, I^-) and voltages (V^+, V^-) during the voltage dip are shown in Fig. 7. Both conventional and unbalance controls inject 1.11 pu of I^+ to ensure delivering the rated real power. However, the uncontrollable current I^- settles at 0.21 pu in the conventional mode, while the

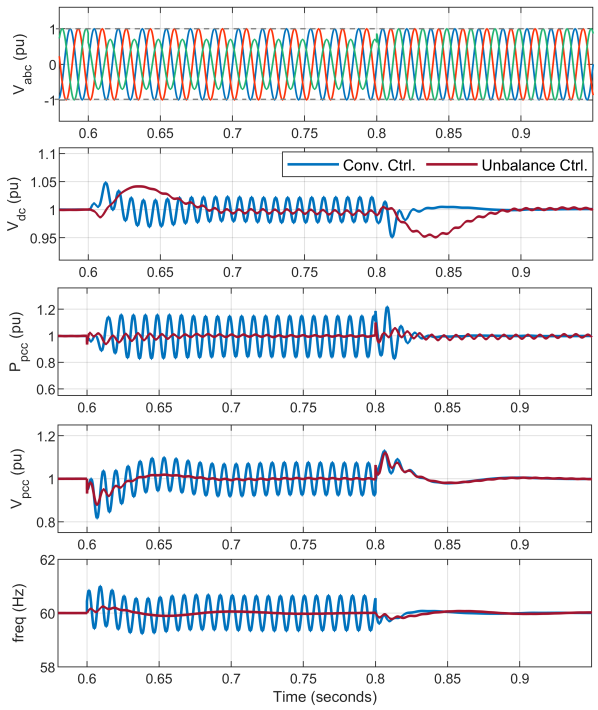

Fig. 6: Case 2: time domain simulation responses of the system due to grid voltage dip at 0.6 sec. From top to bottom, three-phase voltage, dc-link voltage, PCC active power, PCC-bus voltage, and system frequency.

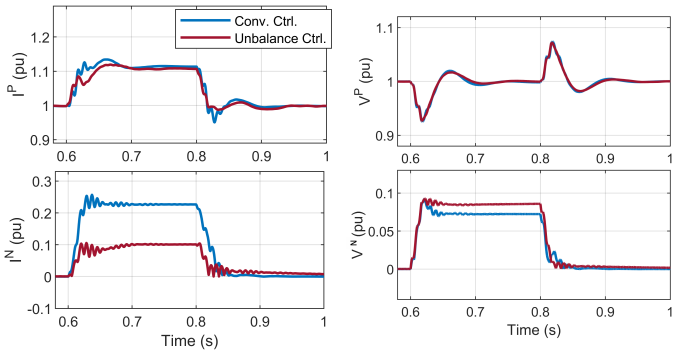

(a) I^+ and I^- (b) V^+ and V^-

Fig. 7: Case 2: dynamic responses of the symmetrical sequence current and voltage components due to grid voltage dip.

controlled I^- is limited at 0.1 pu in the unbalance mode. It is obvious that the effect of the negative-sequence current is influenced by the real power ripples (P_{ripple}). Thus, by setting P_{c2} and P_{s2} in (7) to be zero, the I^- can be limited. Since the ac voltage is regulated, both the convectional and unbalance modes show similar responses of V^+ before and after the disturbance.

V. Conclusion

This paper analyzes the dynamic performance of grid-connected PV system when unbalance VSC control is implemented. In addition to mitigating ripples in the real power and the dc voltage, the control adopts ac and dc-link voltage regulations. The effect of the unbalance control is demonstrated by comparing its dynamic performance with the conventional VSC control. During the fault, the unbalance control improves the system's transients and reduces overcurrents. When the grid voltage is subjected to a phase dip, the unbalance control is not only able to damp out the double frequency ripples in the power, but also to limit the negative-sequence current.

Acknowledgement

The authors wish to acknowledge Prof. Lingling Fan's help for her suggestions.

References

[1] P. Michael and P. Joe, "Impact of ieee 1547 standard on smart inverters," *IEEE PES Industry Technical Support Task Force, Tech. Rep.*, 2018.

[2] G. Kou, L. Chen, P. VanSant, F. Velez-Cedeno, and Y. Liu, "Fault characteristics of distributed solar generation," *IEEE Transactions on Power Delivery*, vol. 35, no. 2, pp. 1062–1064, 2019.

[3] R. Teodorescu, M. Liserre, and P. Rodriguez, *Grid converters for photovoltaic and wind power systems*. John Wiley & Sons, 2011, vol. 29.

[4] S. Alepuz, S. Busquets-Monge, J. Bordonau, J. A. Martínez-Velasco, C. A. Silva, J. Pontt, and J. Rodríguez, "Control strategies based on symmetrical components for grid-connected converters under voltage dips," *IEEE Transactions on Industrial Electronics*, vol. 56, no. 6, pp. 2162–2173, 2009.

[5] L. Fan, H. Yin, and Z. Miao, "A novel control scheme for dfig-based wind energy systems under unbalanced grid conditions," *Electric Power Systems Research*, vol. 81, no. 2, pp. 254–262, 2011. [Online]. Available: https://www.sciencedirect.com/science/article/pii/S0378779610002105

[6] R. Kabiri, D. G. Holmes, and B. P. McGrath, "Control of active and reactive power ripple to mitigate unbalanced grid voltages," *IEEE Transactions on Industry Applications*, vol. 52, no. 2, pp. 1660–1668, 2015.

[7] H.-S. Song and K. Nam, "Dual current control scheme for pwm converter under unbalanced input voltage conditions," *IEEE transactions on industrial electronics*, vol. 46, no. 5, pp. 953–959, 1999.

[8] M. Reyes, P. Rodríguez, S. Vázquez, A. Luna, J. M. Carrasco, and R. Teodorescu, "Decoupled double synchronous reference frame current controller for unbalanced grid voltage conditions," in *2012 IEEE Energy Conversion Congress and Exposition (ECCE)*. IEEE, 2012, pp. 4676–4682.

[9] M. Mirhosseini, J. Pou, B. Karanayil, and V. G. Agelidis, "Resonant versus conventional controllers in grid-connected photovoltaic power plants under unbalanced grid voltages," *IEEE Transactions on Sustainable Energy*, vol. 7, no. 3, pp. 1124–1132, 2016.

[10] R. Teodorescu, F. Blaabjerg, M. Liserre, and P. C. Loh, "Proportional-resonant controllers and filters for grid-connected voltage-source converters," *IEE Proceedings-Electric Power Applications*, vol. 153, no. 5, pp. 750–762, 2006.

[11] L. Fan, *Control and dynamics in power systems and microgrids*. CRC Press, 2017.

[12] A. Yazdani and R. Iravani, *Voltage-sourced converters in power systems: modeling, control, and applications*. John Wiley & Sons, 2010.

[13] A. Alsaif, Z. Miao, and L. Fan, "Comparison of islanding and synchronization for a microgrid with different converter control," in *2019 North American Power Symposium (NAPS)*. IEEE, 2019, pp. 1–6.

[14] E. Afshari, G. R. Moradi, R. Rahimi, B. Farhangi, Y. Yang, F. Blaabjerg, and S. Farhangi, "Control strategy for three-phase grid-connected pv inverters enabling current limitation under unbalanced faults," *IEEE Transactions on Industrial Electronics*, vol. 64, no. 11, pp. 8908–8918, 2017.